On seeding, large-scale wave structure, equatorial spread *F*, and scintillations over Vietnam

Roland T. Tsunoda,[1] Mamoru Yamamoto,[2] Takuya Tsugawa,[3] Thai Lan Hoang,[4] S. Tulasi Ram,[2] Smitha V. Thampi,[5] Ha Duyen Chau,[6] and Tsutomu Nagatsuma[3]

[1] Understanding the day-to-day variability in occurrence of equatorial spread *F* (ESF) remains as a high-priority objective in space weather research. A major difficulty has been an inability to resolve the roles being played by large-scale wave structure (LSWS) and the post-sunset rise (PSSR) of the equatorial *F* layer, in the production of ESF. In this paper, we show conclusively that total electron content (TEC), measured as a function of latitude and longitude, provides clear, routine descriptions of LSWS. Then, together with ionosonde data, we show, for the first time, that while a seed for LSWS can occur in the late afternoon, its amplification takes place mostly during the PSSR. Implications of these findings are discussed in light of existing theories. **Citation:** Tsunoda, R. T., M. Yamamoto, T. Tsugawa, T. L. Hoang, S. Tulasi Ram, S. V. Thampi, H. D. Chau, and T. Nagatsuma (2011), On seeding, large-scale wave structure, equatorial spread *F*, and scintillations over Vietnam, *Geophys. Res. Lett.*, *38*, L20102, doi:10.1029/2011GL049173.

1. Introduction

[2] This paper is the third in a continuing series of reports that address the question, what is the role of large-scale wave structure (LSWS) in the development of equatorial spread *F* (ESF) and equatorial plasma bubbles (EPBs)? (Earlier results are reported by *Thampi et al.* [2009, hereinafter PP1] and *Tsunoda et al.* [2010, hereinafter PP2].) The notion that LSWS arises around the time of the post-sunset rise (PSSR) of the *F* layer, and controls when and where smaller-scale irregularities (in the form of ESF, scintillation, and radar backscatter) develop, was first suggested by *Tsunoda and White* [1981] and resurrected by *Tsunoda* [2005]. But, thus far, very little has been learned about LSWS.

[3] A major obstacle to answering the above question has, in fact, been our inability to measure LSWS properties. This situation, however, was changed recently with the launch of the Communications/Navigation Outage Forecasting System (C/NOFS) satellite [*de La Beaujardière and the C/NOFS Definition Team*, 2004] into a near-equatorial (13° inclination) orbit. By receiving radio signals (150, 400 MHz) from the CERTO beacon on C/NOFS, using a cluster of stations, it is now possible to determine total electron content (TEC) variations as a function of latitude and longitude, and those variations can be interpreted in terms of LSWS (PP1; PP2). An objective of these studies is to uncover the details of the interrelationships among PSSR, LSWS, ESF, and scintillation.

[4] In this paper, we present more information about LSWS, this time from a case study: 9 March 2011. The results are from data collected with beacon receivers at Bac Lieu (9.3°N, 105.7°E; 2.0°N dip latitude), Ho Chi Minh City (10.8°N, 106. 7°E; 3.8°N dip latitude), and Nha Trang (12.3°N, 109.2°E; 5.6°N dip latitude), and from data collected with an ionosonde at Bac Lieu. (These locations are hereafter referred to as BCL, HCM, and NHA.) This study expands on the one-station results from BCL (PP1), and is similar to the cluster experiment conducted in the Pacific sector (PP2). We focus here on measurements made during a time interval, which included two C/NOFS passes; the first coincided with *E*-region sunset (SS_E) during the PSSR, and the second occurred during descent of the *F* layer, when ESF became fully developed. Magnetic activity was very quiet and solar activity moderately high ($F10.7 \sim 140 \times 10^{-22}$ W/m^2/Hz).

2. Results

2.1. PSSR and ESF

[5] Ionograms, taken at 15 min intervals, were used to describe the PSSR and ESF. (See *Saito and Maruyama* [2006] for ionosonde details.) Results are summarized in Figure 1. Contours of constant plasma frequency (f_N) are plotted as a function of virtual height (h') and universal time (UT). Local time (LT) leads UT by 7 hr. Each contour is labeled with its f_N value, which corresponds with a plasma density (N). Examples are $f_N = 3$ MHz ($N \sim 10^5$ el/cm^3) and $f_N = 9$ MHz ($N \sim 10^6$ el/cm^3). Both SS_E and *F*-region sunset (SS_F) are marked by vertical lines. Circles indicate absence of ESF, vertical bars indicate approximate extent in h' of the range spread. Sporadic *E* (E_s) did not appear until 1430 UT.

[6] Behavior on this night was typical of those in which ESF occurs. The PSSR rate (3 MHz contour) maximized around SS_E at a speed of 20 to 30 m/s. This rate is typical for the Vietnam sector; similar speeds of 10 and 20 m/s were measured over BCL in January 2009 (PP1). Averaged model results, derived from ROCSAT satellite data (1999 to 2004), are also similar for this longitude sector and equinoctial months [*Fejer et al.*, 2008]. The occurrence of ESF on this night is consistent with *Saito and Maruyama* [2006],

[1]Center for Geospace Studies, SRI International, Menlo Park, California, USA.
[2]RISH, Kyoto University, Uji, Japan.
[3]National Institute of Information and Communications Technology, Koganei, Japan.
[4]Ho Chi Minh City Institute of Physics, Vietnam Academy of Science and Technology, Ho Chi Minh City, Vietnam.
[5]Physical Research Laboratory, Ahmedabad, India.
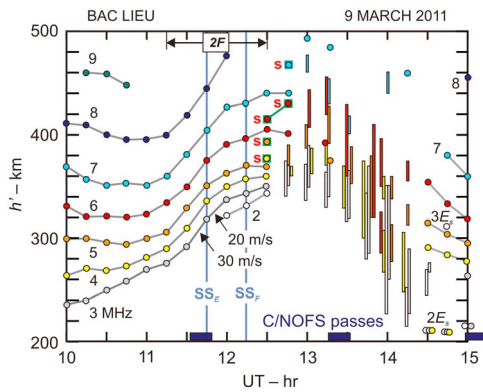[6]Institute of Geophysics, Vietnam Academy of Science and Technology, Hanoi, Vietnam.

Figure 1. Plot of virtual height at several f_N versus UT, over Bac Lieu on 9 March 2011. Black bars indicate times of C/NOFS passes.

Figure 3. (top) Absolute vertical TEC versus longitude and (bottom) the LSWS component, from 1132 UT pass taken at BCL, 9 March 2011.

at least in an averaged sense. Using ionograms from Chumphon (10.7°N, 99.4°E, 3.3° dip latitude) taken in October 2004, when the average sunspot number (SSN) was ~48, and from March and April 2005, when SSN ~ 24, they found that EPBs were produced on nights when $h'(2.5)$ reached a maximum altitude of 330 km, around 1945 LT. They also found that EPBs were not launched on nights when $h'(2.5)$ reached a maximum altitude of 315 km, at a slightly earlier time (1925 LT). In comparison, on 9 March 2011, SSN ~ 56, and $h'(2.5)$ reached a maximum altitude of ~340 km, around 1930 LT. (Effects of a meridional neutral wind on ESF occurrence could not be assessed.)

[7] Development of ESF on this night was also typical. We have some evidence in the form of ionogram signatures, that an upwelling developed over this region. Although multi-reflected echoes (MREs) [*Tsunoda*, 2009] were not observed, satellite traces (STs), (i.e., extraneous near-replicas of main ionogram traces, which indicate LSWS presence [*Tsunoda*, 2008]), were observed. They are indicated in Figure 1 by boxed circles, labeled with the letter s. Inference of an upwelling presence is consistent with the more direct evidence, presented in section 2.2. From Figure 1, ESF started at the base of the *F* layer (lower f_N) and worked its way upward (through higher f_N) toward the *F* peak. Full ESF appeared about an hour later. The disturbance, however, was not long-lived; ESF weakened around 2115 LT (1415 UT) and was essentially gone by 2130 LT (1430 UT).

2.2. Relationship of TEC Measurements to LSWS

[8] The sets of tracks of the ionospheric penetration points (IPPs), assumed to be at 300 km, for the two C/NOFS
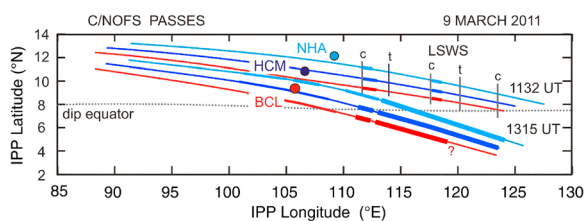

Figure 2. Tracks of the ionospheric penetration points (IPPs) for BCL, HCM, and NHA, for the C/NOFS passes at 1132 and 1315 UT, 9 March 2011.
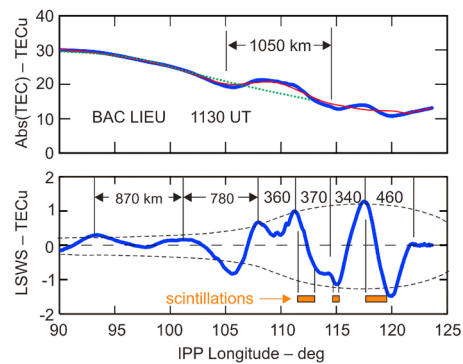
passes, are shown plotted in Figure 2, as a function of geographical latitude and longitude. The red curves are for BCL, purple for HCM, and blue for NHA. Notice that while a description of TEC variation is available as a function of longitude, along an IPP track, the three tracks provide information about variations as a function of latitude. Descriptions of receiver design and data analysis are given by *Yamamoto* [2008] and PP1. TEC is derived from the differential phase between the two received signals. The processing, described by PP1, has been extended to now provide the absolute, not just relative, TEC. (Relative TEC estimates were used by PP1 and PP2.) The method and details that show how accurate estimates of absolute TEC are obtained, are presented by S. Tulasi Ram et al. (On the application of differential phase measurements to study the zonal large-scale wave structure (LSWS) in the ionospheric electron content, submitted to *Radio Science*, 2011).

2.2.1. Background TEC Variations

[9] A plot of absolute vertical TEC (VTEC) from the first pass is presented in Figure 3 (top). For our purposes here, we simply consider the largest-scale variations to be part of the background ionosphere. Most apparent is a west-to-east decrease in VTEC, from 30 TECu (at 90°E longitude), to less than 15 TECu (at 125°E longitude), where 1 TECu = 10^{16} el/m². This decrease is similar to that of the equatorial *F* layer found around sunset in Jicamarca incoherent-scatter (IS) radar measurements [*Farley et al.*, 1967]. At slightly smaller spatial scales, there is a 1000-km-scale enhancement of ~4 TECu, between 105°E and 114.5°E longitudes.

2.2.2. LSWS Component

[10] Residual variations in VTEC, with spatial scales less than ~1000 km, are plotted in Figure 3 (bottom). This curve was obtained by subtracting a 2.5 min running average (red) curve from the blue curve; both are shown in the top panel (although the red curve is difficult to see, where the two curves coincide). The running average is intended to match a zonal distance of ~1000 km (PP1). (This zonal distance decreases to ~500 km at low elevation angles, as discussed by Tulasi Ram et al. (submitted manuscript, 2011).) The curve in the bottom panel displays wavelike variations over most of the longitude sector shown. Its amplitude, however, is not uniform; instead, it is small (large) to the west (east) of BCL (105.7°E). Although we are not certain of its significance, the smallest amplitudes here (~0.1 to 0.3 TECu) appear comparable to the largest that were observed during
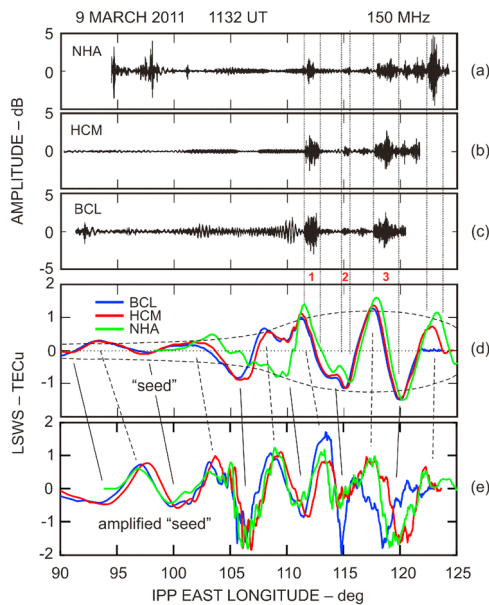
Figure 4. Amplitude of VHF signal received at (a) BCL, (b) HCM, and (c) NHA, on 9 March 2011.

2009, for a similar LT. The largest amplitude in Figure 3 is ~1 TECu.

2.2.3. Zonal Wavelengths

[11] Perhaps a first indication that residual VTEC variations are related to LSWS comes from observed zonal wavelengths, 340 to 870 km in Figure 3 (bottom). These wavelengths are comparable to those determined by IS radar [*Tsunoda and White*, 1981] and satellite probes [e.g., *Singh et al.*, 1997]. The finding that zonal wavelength decreased from west to east during one pass, however, is new and not expected, if we envision excitation and development of LSWS to be uniform over 35° in longitude. On the other hand, variability would be expected, if seeding and amplification are more localized.

2.2.4. Magnetic Alignment

[12] A stronger indication of a VTEC-LSWS relationship is the finding that both VTEC residuals and LSWS are aligned with geomagnetic field ($\vec{B}$) lines. PP1 showed, using beacons on equatorial- and polar-orbiting satellites, that VTEC varied more rapidly in the zonal, rather than meridional, direction. PP2 showed VTEC depletions to be aligned along $\vec{B}$ lines, by using a cluster of three TEC receivers in the Pacific sector, which are spaced in latitude as well as longitude. Results similar to those of PP2 were found here, as shown in Figure 4d, where we have plotted the VTEC residual curves from BCL, HCM, and NHA. Given that the declination of $\vec{B}$ is near zero in this sector, alignment along $\vec{B}$ is equivalent to a close alignment in longitude. This is indeed the case for the crests and depletions in the 110° to 122°E sector. From IPP tracks that were spaced over 3° in latitude, we conclude that alignment with $\vec{B}$ occurred over at least 300 km.

2.2.5. Alignment of LSWS and Scintillations

[13] Our most convincing evidence that VTEC residual variations are directly related to LSWS are simultaneous measurements of amplitude scintillations that were imposed on the same signals used to derive VTEC. The plots of signal amplitude at 150 MHz for the first pass, after detrending, are

shown in Figures 4a–4c. (We ignore signal perturbations that were not found in all three curves.) Of interest are three scintillation patches, which we have labeled 1, 2, and 3. They are aligned not only in longitude (hence, $\vec{B}$), but also with the west walls of VTEC depletions (follow the vertical lines to Figure 4d). This alignment is identical to that found between radar backscatter, which are collocated with EPBs, and west walls of upwellings, which are associated with LSWS [*Tsunoda and White*, 1981; *Tsunoda*, 1983]. *Tsunoda* [1983] further showed that secondary EPBs develop along the west walls. We, therefore, feel that we now have a sound basis for interpreting depletions in a VTEC residual curve in terms of upwellings associated with LSWS. (We note that TEC variations can become distorted when EPBs appear; but this would be accompanied by the appearance of strong, but not weak, scintillations, as is the case at 1132 UT.)

2.3. Seeding, PSSR, and LSWS Growth

[14] For the remainder of this paper, we focus on the seeding and amplification of LSWS. PP1 presented evidence that LSWS can appear before SS_E and become amplified with time. In one of the datasets, LSWS was detected when the solar zenith angle (χ) was only 86.6° (PP1); in other words, even before ground sunset. Here (Figure 4d), we present another example. At 1135 UT, χ was 85° at an IPP location (12°N, 93°E), where LSWS was detected. This observation clearly occurred before the PSSR. Growth in LSWS amplitude with time is evident by comparing Figure 4d to Figure 4e. We can see that the seed VTEC depletion, observed at 98°E at the time of the first pass, had grown in amplitude by the time of the second pass. In addition, the two VTEC depletions near the center of the panels have continued to grow. On the other hand, the large VTEC depletion located around 120°E has become complex and structured. Hence, we appear to have a situation in which LSWS amplitude was smaller prior to SS_E and larger after SS_E. In other words, Figures 4d and 4e confirm the finding by PP1 that LSWS appeared well before SS_E and grew temporally during the SS_E period. The growth of LSWS during PSSR is identical to that found with the ALTAIR IS radar [*Tsunoda and White*, 1981].

[15] A new feature, not found by PP1, is the variation in LSWS amplitude with longitude (Figure 4d). A similar feature was observed, however, on 12 September 2009 in the Pacific sector (PP2). In both cases, small LSWS amplitudes were found to the west and large amplitudes were found to the east. The transition distance (from small to large amplitudes) was similar, 8° in longitude on 12 September 2009 and 12° on 9 March 2011. In PP2's dataset, perturbation amplitude to the west did not grow at all, whereas growth did occur to the east. This behavior was interpreted in terms of localized seeding in one region but not the other, which occurred on a night when the PSSR was absent.

[16] Viewing Figures 4d and 4e together, we envision a similar interpretation, in terms of seeding, but with presence of a more substantial PSSR than found for 12 September 2009. We suggest that strong, localized seeding occurred to the east of 105°E longitude, and that weaker seeding occurred to the west of that longitude. The weaker seed could have been associated with another localized event, or it could have been associated with a ubiquitous background. This notion is appealing in that the observations of different

wavelengths can be explained in terms of different seed sources. In PP2's case, PSSR was essentially zero, which explains why LSWS did not appear over Pohnpei, whereas, a moderate PSSR occurred over BCL, which explains the LSWS amplification over Vietnam. Interestingly, small-scale fluctuations are absent in the curves to the west of 101°E, but are present to the east of that longitude. The implication is that the seeding and/or amplification properties were different in the two longitude sectors on 9 March 2011.

3. Discussion

[17] We have extracted two key results from this case study. First, we have shown that TEC measurements using a radio beacon on an equatorial-orbiting satellite can provide clear routine descriptions of LSWS and the scintillations that develop within upwellings and EPBs. In fact, our demonstration that scintillation patches are spatially coincident with the west walls of VTEC depletions, provides the most convincing evidence that VTEC depletions are directly related to upwellings in LSWS. And, second, we can now say with confidence that seeds for LSWS can appear in the late afternoon, when χ is as small as 85°. Moreover, indications are growing that both seeding and amplification may be patchy and more localized in longitude than we have realized to date.

[18] The basic scenario for LSWS excitation has not been changed by the results of this study. That is, seeding could still occur from a sequence of events, beginning with the excitation of atmospheric gravity waves (AGWs) in the troposphere or lower thermosphere, their propagation up to the thermosphere, and the transfer of AGW wind perturbations via neutral-ion coupling to the plasma at the base of the F layer (see *Tsunoda* [2010a, 2010b, 2010c] for details). In fact, the findings that seeding and amplification are more localized and not uniform in longitude are consistent with recent, more realistic models for AGW excitation. For example, *Vadas and Fritts* [2004] used an ensemble of 30 spatially and temporally localized, vertical body forces, which occur randomly within a mesoscale region. The individual convective "plumes" that result can have different diameters, depths, and strengths. And, because rapid temporal variations are requisite for strong AGW excitation, we have good reason to expect LSWS to appear as we have described.

[19] The existence of a late afternoon seed answers a few questions and raises others. We can say that late-afternoon seeds are not likely a consequence of the PSSR, in agreement with PP1 and PP2. We can also conclude that the zonal wavelength of LSWS is not likely controlled by the collisional-shear instability [*Hysell and Kudeki*, 2004], which selects a wavelength based on the velocity-shear scale size. The reason is that these shears occur on the night side, but not on the day side of the PSSR.

[20] A concern with late-afternoon seeding is the possibility of loading of the F-region dynamo by a sunlit E region [e.g., *Tsunoda*, 2007; PP1]. Results from *Crain et al.* [1993] suggest that this would not be a problem. If we use Figure 3 of *Crain et al.* [1993], the loading factor, given by (Σ_P^F/Σ_P^E) $[1 + \Sigma_P^F/\Sigma_P^E]^{-1}$, would change only slightly, from 0.7 near noon, to 0.8 when χ is 85°; if so, the role of the E region would be minor at all times. On the other hand, they did not

examine what happens on $\vec{B}$ lines whose apex altitude is at the base of the F layer, where seeding is believed to occur [*Tsunoda*, 2010a, 2010b, 2010c]. Presumably, near the base of the F layer, E-region effects are manifested in the form of westward zonal drift [*Anderson and Mendillo*, 1983; *Crain et al.*, 1993]. If so, the finding that the zonal drift of LSWS can be nearly zero [*Tsunoda*, 2005] suggests that LSWS may be situated near the transition altitude, from westward to eastward flow. An implication could be that E-region dynamo may be important. Clearly, further study of this topic is needed.

[21] Finally, our finding, that the growth rate of LSWS can be substantial during the PSSR, suggests a need for an instability process, perhaps the interchange instability driven by the PSSR. When considering this possibility, we should keep in mind that the domain of interest is $kL < 1$ (not $kL > 1$), where $k = 2\pi/\lambda$, $\lambda \approx 400$ km, and $L \approx 20$ km [e.g., *Tsunoda and White*, 1981].

References

Anderson, D. N., and M. Mendillo (1983), Ionospheric conditions affecting the evolution of equatorial plasma depletions, *Geophys. Res. Lett.*, *10*, 541, doi:10.1029/GL010i007p00541.

Crain, D. J., R. A. Heelis, and G. J. Bailey (1993), Effects of electrical coupling on equatorial ionospheric plasma motions: When is the F region a dominant driver in the low-latitude dynamo?, *J. Geophys. Res.*, *98*, 6033, doi:10.1029/92JA02195.

de La Beaujardière, O., and the C/NOFS Definition Team (2004), C/NOFS: A mission to forecast scintillations, *J. Atmos. Sol. Terr. Phys.*, *66*, 1573, doi:10.1016/j.jastp.2004.07.030.

Farley, D. T., J. P. McClure, D. L. Sterling, and J. L. Green (1967), Temperature and composition of the equatorial ionosphere, *J. Geophys. Res.*, *72*, 5837, doi:10.1029/JZ072i023p05837.

Fejer, B. G., J. W. Jensen, and S.-Y. Su (2008), Quiet time equatorial F region vertical plasma drift model derived from ROCSAT-1 observations, *J. Geophys. Res.*, *113*, A05304, doi:10.1029/2007JA012801.

Hysell, D. L., and E. Kudeki (2004), Collisional shear instability in the equatorial F region ionosphere, *J. Geophys. Res.*, *109*, A11301, doi:10.1029/2004JA010636.

Saito, S., and T. Maruyama (2006), Ionospheric height variations observed by ionosondes along magnetic meridian and plasma bubble onsets, *Ann. Geophys.*, *24*, 2991, doi:10.5194/angeo-24-2991-2006.

Singh, S., F. S. Johnson, and R. A. Power (1997), Gravity wave seeding of equatorial plasma bubbles, *J. Geophys. Res.*, *102*, 7399, doi:10.1029/96JA03998.

Thampi, S. V., M. Yamamoto, R. T. Tsunoda, Y. Otsuka, T. Tsugawa, J. Uemoto, and M. Ishii (2009), First observations of large-scale wave structure and equatorial spread F using CERTO radio beacon on the C/NOFS satellite, *Geophys. Res. Lett.*, *36*, L18111, doi:10.1029/2009GL039887.

Tsunoda, R. T. (1983), On the generation and growth of equatorial backscatter plumes. 2. Structuring of the west walls of upwellings, *J. Geophys. Res.*, *88*, 4869, doi:10.1029/JA088iA06p04869.

Tsunoda, R. T. (2005), On the enigma of day-to-day variability in equatorial spread F, *Geophys. Res. Lett.*, *32*, L08103, doi:10.1029/2005GL022512.

Tsunoda, R. T. (2007), Seeding of equatorial plasma bubbles with electric fields from an E_s-layer instability, *J. Geophys. Res.*, *112*, A06304, doi:10.1029/2006JA012103.

Tsunoda, R. T. (2008), Satellite traces: An ionogram signature for large-scale wave structure and a precursor for equatorial spread F, *Geophys. Res. Lett.*, *35*, L20110, doi:10.1029/2008GL035706.

Tsunoda, R. T. (2009), Multi-reflected echoes: Another ionogram signature of large-scale wave structure, *Geophys. Res. Lett.*, *36*, L01102, doi:10.1029/2008GL036221.

Tsunoda, R. T. (2010a), On seeding equatorial spread *F* during solstices, *Geophys. Res. Lett.*, *37*, L05102, doi:10.1029/2010GL042576.

Tsunoda, R. T. (2010b), On seeding equatorial spread *F*: Circular gravity waves, *Geophys. Res. Lett.*, *37*, L10104, doi:10.1029/2010GL043422.

Tsunoda, R. T. (2010c), On equatorial spread *F*: Establishing a seeding hypothesis, *J. Geophys. Res.*, *115*, A12303, doi:10.1029/2010JA015564.

Tsunoda, R. T., and B. R. White (1981), On the generation and growth of equatorial backscatter plumes: 1. Wave structure in the bottomside *F* layer, *J. Geophys. Res.*, *86*, 3610, doi:10.1029/JA086iA05p03610.

Tsunoda, R. T., D. M. Bubenik, S. V. Thampi, and M. Yamamoto (2010), On large-scale wave structure and equatorial spread *F* without a post-sunset rise of the *F* layer, *Geophys. Res. Lett.*, *37*, L07105, doi:10.1029/2009GL042357.

Vadas, S. L., and D. C. Fritts (2004), Thermospheric responses to gravity waves arising from mesoscale convective complexes, *J. Atmos. Sol. Terr. Phys.*, *66*, 781, doi:10.1016/j.jastp.2004.01.025.

Yamamoto, M. (2008), Digital beacon receiver for ionospheric TEC measurement developed with GNU radio, *Earth Planets Space*, *60*, e21.

H. D. Chau, Institute of Geophysics, Vietnam Academy of Science and Technology, 18 Hoang Quoc Viet, Cau Giay, Hanoi, Vietnam.

T. L. Hoang, Ho Chi Minh City Institute of Physics, Vietnam Academy of Science and Technology, 01 Mac Dinh Chi St., District 1, Ho Chi Minh City, Vietnam.

T. Nagatsuma and T. Tsugawa, National Institute of Information and Communications Technology, 4-2-1 Nukui-kita, Koganei, Tokyo 184-8795, Japan.

S. V. Thampi, Physical Research Laboratory, Ahmedabad 380 009, India.

R. T. Tsunoda, Center for Geospace Studies, SRI International, 333 Ravenswood Ave., Menlo Park, CA 94025, USA. (tsunoda@sri.com)

S. Tulasi Ram and M. Yamamoto, RISH, Kyoto University, Gokasho, Uji, Kyoto 611-0011, Japan.